

Quantitative and qualitative performance of density functional theory rationalized by reduced density gradient distributions

Ageo Meier de Andrade , Jolla Kullgren , and Peter Broqvist ^{*}
Department of Chemistry - Ångström Laboratory, Uppsala University, Sweden



(Received 16 April 2020; revised 22 June 2020; accepted 24 June 2020; published 13 August 2020)

We evaluate the qualitative and quantitative accuracy of various flavors of density functionals with and without accounting for dispersion corrections. Our test system is nickel in the form of bulk, surfaces, and nanoparticles for which we compute structural properties, bulk cohesive energies, surface energies, and work functions and compare to experimental data. We find that the inclusion of any dispersion, either by an *a posteriori* correction or by a self-consistent treatment by explicitly computing the nonlocal correlation contribution to the total energy, has a significant effect on the calculated properties and improves the quantitative comparison to experiments. Besides the quantitative agreement, we also investigate qualitative features by comparing Wulff shapes of metal nanoparticles as obtained using the different density functionals. We find that all tested functionals predict similar Wulff shapes for nickel nanoparticles but still have some small differences. These results show that the relative energies calculated using the semilocal GGA and meta-GGA functionals, with and without dispersion, are quite similar. Our findings can also be generalized to other systems when rationalized in terms of the computed reduced density gradients. We find that the distribution of reduced density gradients in a material is correlated to the steepness of the exchange enhancement factor and propose that this information can be used as a quantitative guide when it comes to picking the most appropriate density functional for specific target systems as well as when it comes to extrapolating DFT data to predict experiments.

DOI: [10.1103/PhysRevB.102.075115](https://doi.org/10.1103/PhysRevB.102.075115)

I. INTRODUCTION

The power of electronic structure calculations based on the density functional theory (DFT) to guide scientists by capturing and explaining trends in classes of materials, e.g., metals, oxides, or even molecular materials, cannot be underestimated. DFT has, therefore, become an invaluable tool in modern materials science. However, quantitative agreement with experiments is often difficult to reach, and the predictive power of DFT can, therefore, be questioned, in particular for complex materials when combinations of different chemical bonding occur in the same material [1]. As a result, a plethora of various density functionals have been proposed in the literature, see, e.g., the review by Mardirossian and Head-Gordon [2], where about 200 density functionals were benchmarked towards a set of nearly 5000 data points. Still, however, when it comes to choosing the right one, it is most often up to the experience of the modeler to identify the functional which best captures the particularities of the target system or target properties. As a consequence, the optimal choice of density functional often varies between different research areas.

One area where DFT have been extensively used is heterogeneous catalysis [3]. Here, the search for better and more efficient catalysts has been a long, and still ongoing, enduring quest. A good catalyst in this context has both high reactivity, and high selectivity, with both targets preferably reached at a low cost. Metallic nanoparticles have been shown to serve as excellent catalysts for many chemical reactions, partly because their properties can be tailored by varying their size, shape, and composition, by alloying or doping [4]. Most often, the metals of choice are the noble metals palladium or platinum, but also nickel and other late transition metals are used. Given the high cost of these metals (especially the former), the trend in the field is to make “every atom count,” either by reducing particle sizes further, or, by embedding active catalytic centers in a cheaper material. This has increased the interest when it comes to understanding, and predicting, the atomic-scale structure of active catalysts [4,5]. If we want to understand the relationship between surface structure and the property of a material, experiments alone are often too obtuse, and here theory could play a vital role, given that sufficient accuracy can be reached.

From a theoretical point of view, freestanding and supported nanoparticles are difficult to treat, not least due to their inhomogeneous electron density [4]. For example, in the core of the nanoparticle, there is a metallic bulklike structure with a slowly varying electron density. Close to the surface, the charge density changes abruptly. Ideally, these different chemical environments should be described with the same accuracy. However, this turns out to be quite challenging. In the context of DFT, many such variations in electron density can be

^{*}peter.broqvist@kemi.uu.se

conveniently characterized using the reduced electron density gradient [6,7]. From experience, it is known that the so-called local density approximation LDA [8] behaves quite well for systems where the electron density varies slowly (small reduced density gradients), such as for metals. In LDA, the exchange-correlation energy is calculated solely from the behavior of a homogeneous electron gas. However, for systems showing abrupt changes in electron density, i.e., systems with high reduced electron density gradients, such as in the case for many molecules, more complex descriptions are needed. For such systems, the inclusion of density gradients, as done in the various generalized gradient approximations to the LDA (the so-called GGA functionals), improves the description. In the materials science community, the semilocal GGA functional as proposed by Perdew-Burke-Ernzerhof, the so-called PBE functional [9,10], has become very popular, as it gives a satisfactory description of both matters in the condensed phase, as well as for molecules. Using the PBE functional form as a starting point, there have been further developments to increase the quantitative accuracy for solids (PBEsol [11]) and molecules (revised PBE, RPBE [12]). By adding further flexibility when treating the exchange contribution of the system, new functional forms can be reached. For example, adding the kinetic energy density as an additional semilocal information besides the electron density gradient leads to the so-called meta-GGAs. These functionals are often constructed with some specific system or material class in mind. Some examples that target condensed matter systems are the functional proposed by Tao-Perdew-Staroverov-Scuseria (TPSS) [13] and the strongly constrained and appropriately normed (SCAN) density functional [14].

Despite the success of DFT, especially in terms of accuracy *versus* computational efficiency, as found for the semilocal GGA functionals, it does not account for dispersion interactions. This shortcoming can, however, be rectified either by adding an *a posteriori* correction to the total energy or by self-consistently accounting for nonlocal correlation already in the density functional. Here, for the *a posteriori* methods, the DFT-Dn methods by Grimme, with $n = 1-3$, have become very popular [15-17]. However, there exist also other methods to correct the DFT total energy for lacking dispersion, such as the Tkatchenko and Scheffler method [18], the uMBD [19] and the XDM [20]. Examples of the self-consistent approaches are the so-called vdW-DF [21] class of density functionals, the rVV10 method [22], and the self-consistent implementation of the Tkatchenko and Scheffler method [23]. While these corrections are modular and can be added to in principle any density functional, it is important to note that from a theoretical point of view, the inclusion of nonlocal correlation has to be compensated by a physically correct treatment of the exchange energy.

The current development in density functionals has inspired us to investigate their performance for different systems with the aim to obtain a general understanding of when to use which functional based on the behavior of the electron density. In this study, we have focused on a single element system (nickel, Ni) but in various forms. We start with different bulk phases and thereafter increase the complexity of the charge density by also looking at atoms and surfaces. Thus, the low reduced density gradient domain is investigated by

studying the fcc and bcc bulk phases of Ni. The medium range is investigated by studying surface properties, which indeed are essential features of metallic nanoparticles. High reduced density gradients are covered by computations on the Ni atom. For the bulk and surfaces, we evaluate structural and energetic properties, as well as the accuracy given by the functionals, both from a quantitative and a qualitative point of view. In our comparisons, we use the PBE density functional as a base line and discuss our results in the light of changes from this functional form. More specifically, our tests comprise to commonly used functionals in materials science starting from LDA, three semilocal GGAs (PBE, PBEsol, and RPBE) and one meta-GGA (SCAN). We account for dispersion interactions through the use of the Grimme's D3 method and three variations of vdW-DF functionals (vdW-DF-cx, optPBE-vdW, and revPBE-vdW). Additionally, we investigate the inclusion of dispersion interactions for SCAN through the rVV10 method (SCAN-rVV10 functional).

This paper is outlined as follows: First, in Sec. II, we give a short theoretical background of the different density functionals tested in this study motivating our choice of functionals and approach of analysis. Thereafter, in Sec. III, we give the details concerning the methods and models. In the following Sec. IV, we evaluate the selected functionals by comparing the results with well defined experimental observables and rank them according to their overall performance, both concerning their quantitative as well as qualitative performance. Later on, in Sec. IV, we go one step further and perform a density functional analysis in terms of the reduced density gradient as an attempt to rationalize and generalize our results. Section V concludes the paper.

II. THEORETICAL BACKGROUND

In this section, we recapitulate some theory behind the different functionals considered in this study necessary to motivate our approach of analysis. We focus on the functional form and the exchange enhancement factor $F_x(s)$ for the different GGAs. We discuss how $F_x(s)$ needs to be modified to increase the accuracy of different classes of materials (and molecules). In addition to the so-called semilocal density functionals, we also discuss the role of the exchange enhancement factor $F_x(s)$ in dispersion corrected density functionals, either by the use of an *a posteriori* correction using a pair-wise force-field description (see, e.g., Ref. [17]) or explicitly by accounting self-consistently for the nonlocal correlation (see, e.g., Ref. [24]).

The core of density functional theory, and what in the end determines the accuracy after all technical details have been solved, is how to calculate the exchange-correlation energy contribution E_{XC} . One useful concept when classifying different functionals is the so-called Perdew's Jacob's ladder [25]. Each rung corresponds to an improved description towards the goal of reaching chemical accuracy. The simplest approach to DFT, which is also the first rung in Perdew's Jacob's ladder, is to calculate E_{XC} through a local description of the electron density, also known as LDA [8].

GGA density functionals correspond to step 2 on Jacob's ladder and are referred to as semilocal when it comes to its density dependence. GGAs are the most commonly used

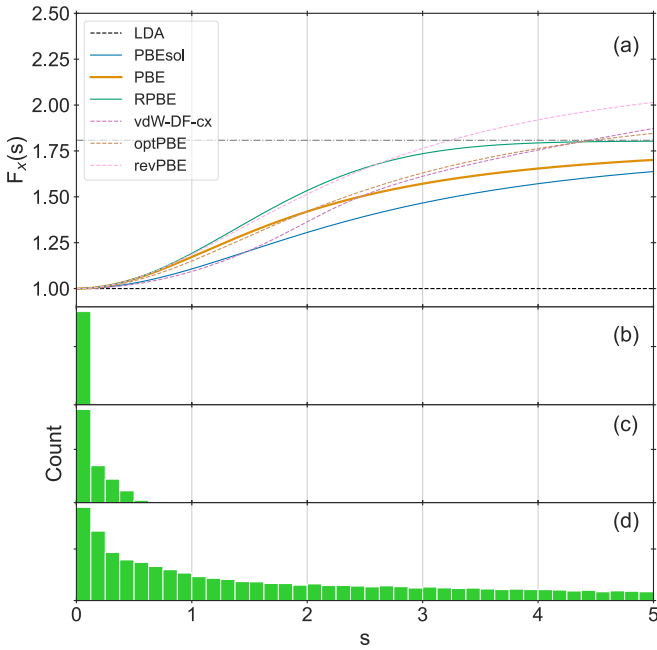


FIG. 1. (a) $F_x(s)$ for various density functionals. Typical s values calculated using PBE for (b) an fcc metal, (c) a metal surface, and (d) an atom.

functionals in DFT, and they have the following general form:

$$E_{XC}^{GGA} = \int d\mathbf{r} \rho(\mathbf{r}) f[\rho(\mathbf{r}), \nabla\rho(\mathbf{r})]. \quad (1)$$

The function $f[\rho(\mathbf{r}), \nabla\rho(\mathbf{r})]$ is called the exchange enhancement factor, often written as $F_x(s)$, i.e., expressed as a function of the reduced density gradient $s[\rho(\mathbf{r})]$ defined as:

$$s[\rho(\mathbf{r})] = \frac{1}{2(3\pi^2)^{1/3}} \frac{|\nabla\rho(\mathbf{r})|}{\rho^{4/3}(\mathbf{r})}. \quad (2)$$

$F_x(s)$ comes in many forms, each corresponding to a specific GGA density functional. In this work, we have chosen a limited set of these and focused on functionals that are commonly used in the field of materials science. These are, with a few exceptions, all based on the nonempirical class of functionals proposed by Perdew, Burke, and Ernzerhof, the so-called PBE density functional [9,10]. Given the importance and vast experience gained from DFT calculations utilizing the PBE density functional, the behavior of PBE will serve as a baseline in the discussion below when it comes to possible modifications of $F_x(s)$ to improve the accuracy of certain computed properties for specific classes of systems.

The exchange enhancement factor of the PBE functional is expressed as

$$F_x^{\text{PBE}}(s) = 1 + \kappa - \kappa / (1 + \mu s^2 / \kappa), \quad (3)$$

where κ and μ are obtained from physical constraints and ensures a continuous function between the limits of $s = 0$ (LDA) and the high s values (the so-called Lieb-Oxford limit [26]). Figure 1(a) shows a plot of $F_x^{\text{PBE}}(s)$ in the range of $0 \leq s \leq 5$. Typical s values for a bulk metal, a metal surface, and a metal atom are given in Fig. 1(b), Fig. 1(c), and Fig. 1(d), respectively.

For the condensed matter, Perdew *et al.* continued working with the same expression as for PBE, but used other constraints when it comes to the fitting of the parameter μ in Eq. (3), still keeping κ the same. This functional is called PBEsol [11], and the $F_x^{\text{PBEsol}}(s)$ is shown and compared to $F_x^{\text{PBE}}(s)$ in Fig. 1(a). The s dependence in $F_x^{\text{PBEsol}}(s)$ is weaker, which is shown to greatly improve many computed properties of systems with low to medium ranges of s values. The calculated properties related to atoms and molecules are worse, making, for example, atomization energies highly inaccurate, as are energies related to molecular adsorption on solid surfaces [11].

For molecules and atoms, which commonly display higher s values [cf., Figs. 1(c) and 1(d)], Hammer *et al.* proposed a new functional form to improve adsorption energies on metal surfaces. As can be seen in Fig. 1(a), the $F_x^{\text{RPBE}}(s)$ now displays a faster increase in comparison to $F_x^{\text{PBE}}(s)$ at smaller s values, which has been shown to improve the description of, for example, atomization energies and molecular adsorption energies with the cost of a less accurate description of the condensed matter [12].

Local and semilocal functionals do not account for long-range dispersion interactions. To properly account for them, we need to compute the nonlocal correlation, which requires many-body theory and is found in much more computationally expensive methods, such as the random phase approximations (RPA, last rung in Jacob's ladder) [27]. In practice, however, dispersion interactions can be added to the DFT energy and be effectively accounted for with an *a posteriori* correction, using a force-field approach, or in a self-consistent manner. One common semiempirical formalism proposed and developed by Grimme and co-workers is called DFT-Dn method [15–17], where $n = 1–3$ represents different versions of dispersion corrections. In this work, we have focused on the D3 version, which uses a force-field accounting for two- and three-body interactions, added directly to the semilocal GGAs total energies [17].

When adding nonlocal correlation effects explicitly into the density functional, a common way is to use a kernel approach, as done in either the Rutgers-Chalmers family (vdW-DF [21]) or that of the VV10 [28] and the rVV10 methods [22]. These approaches are appealing as they aim at solving the core of the problem by building a model that allows for the direct computation of the nonlocal correlation energy based on the ground state density. While many approaches here uses the same kernel, i.e., dispersion description, they differ in the exchange part, i.e., the form of the exchange enhancement factor. The effort lead by the Rutgers-Chalmers team follows the principles of Perdew and co-workers of having an exchange functional that fulfill certain physical constraints, e.g., vdW-DF [21], and the later developed vdW-DF-cx [29], where cx stands for consistent exchange. Other routes use an empirical approach by fitting the exchange functional $F_x(s)$ to best reproduce a test set of different hydrogen-bonded and vdW-bonded molecular systems (the S22 dataset [30]) and is referred to the “opt” family of vdW-DF functionals [31,32]. The optPBE-vdW functional shows promising behavior for many types of systems, and resembles the $F_x^{\text{PBE}}(s)$ to 94.4%, with the remaining part resembling $F_x^{\text{RPBE}}(s)$, cf., Fig. 1(a) [32].

The third rung of Jacob’s ladder comprises the meta-GGA formalism, which allows for further flexibility in the enhancement factor when computing the exchange contribution to the total energy of the system [13]. In the current work, we have tested the SCAN density functional [14], which has been constructed to satisfy all known exact constraints that a meta-GGA can have. To account for nonlocal correlation effects, SCAN can be used together with a self-consistent vdW model to improve the description, in particular for long-range interactions as the inclusion of the kinetic energy density in principle should handle mid-range dispersion interactions. Here, the most common implementation used in conjunction with SCAN is the rVV10 dispersion correction, the so-called SCAN-rVV10 density functional [33].

III. COMPUTATIONAL METHODS

A. Electronic structure method

The electronic structure calculations presented in this work were performed within the framework of spin-polarized density functional theory in the implementation with plane waves and pseudopotentials using the Vienna *ab initio* simulation package (VASP) [34–37]. Pseudopotentials of the projected augmented wave (PAW) type, as proposed by Blöchl, were used in all calculations [38,39]. In the calculations, we explicitly treated Ni $4s^23d^8$ as valence electrons. The pseudopotentials were obtained from the VASP library and are generated using the semilocal PBE density functional, except for the LDA calculations, where LDA generated PAW potentials were used. For consistency, we used the same pseudopotentials in all calculations at the semilocal and meta-GGA density functional level of theory, which may affect the results when compared to all-electron calculations. We believe that changing the pseudopotential would hamper the comparison between the different functionals made in this study. Nonspherical contributions from the gradient corrections inside the PAW spheres were included in all calculations.

Structural optimizations of both unit cells (for bulk systems) and ionic positions (for all systems) were performed using the conjugate gradient algorithm [40], where the cell and ionic relaxation were continued until all components of the stress tensor were less than 0.01 kBar, and the force on each atom was less than 0.01 eV/Å. To speed up electronic convergence during our geometry optimizations, we allowed smearing of the electronic states of 0.2 eV using the Methfessel-Paxton method [41]. All geometry optimizations were followed by single-point calculations, where the electronic states instead were smeared (0.2 eV) using the tetrahedron method with Blöchl corrections [42] for the partial occupancies of the wave function to improve the accuracy of the final electronic structure. The Brillouin zone was sampled using a $16 \times 16 \times 16$ \mathbf{k} -points mesh for the bulk system. For the slabs, we used a mesh of $16 \times 16 \times 1$ \mathbf{k} -points, with the c direction being normal to the surface. In all calculations, we used a plane wave energy cutoff of 600 eV.

We validated our choices by performing tests on selected properties using the vdW-DF-cx functional. Lately, it has been noted that for many systems, hard pseudopotentials and high cutoff energies are needed to converge properties calculated

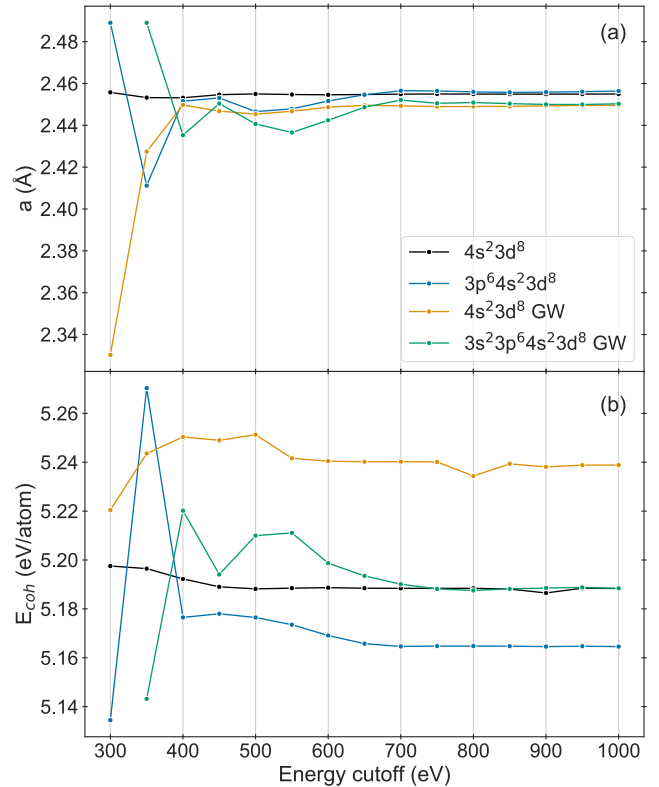


FIG. 2. Calculated properties for different energy cutoffs and different pseudopotentials. (a) shows the lattice constant for fcc Ni, and (b) shows the cohesive energy for fcc Ni. The orange and green lines are obtained using recommended pseudopotentials for GW calculations in VASP, which generally are harder than the standard ones.

using the vdW-DF type of functionals, see, e.g., Kebede *et al.* studying crystalline hydrates [43], Granhed *et al.* studying BaZrO_3 [44], and Vlasisvljevich *et al.* studying metal-organic frameworks [45]. In these studies, cutoff energies up to 1600 eV were used and were deemed necessary to converge certain properties. We tested cutoff energies in the range of 300–1000 eV and verified that 600 eV is sufficient. It is also known that a tighter FFT grid is necessary in order to converge certain properties with the SCAN functional [46]. For all functionals we employed an augmented grid for the representation of the pseudo-orbitals. Our tests revealed that no significant changes are expected in computed properties studied herein for higher cutoff energies and/or harder pseudopotentials (cf., Fig. 2) or tighter FFT grid.

B. Structural models

To investigate how DFT describes bulk metals, we studied the fcc and bcc phases of Ni. These were modelled using primitive unit cells. Low Miller index fcc Ni surfaces, described using a slab model in the supercell approach, were chosen to test surface properties. For each functional, the slab models were built from the corresponding optimized bulk fcc Ni structures at the various levels of theory. The slabs are seven atomic layers thick and have one atom per layer in conjunction with a vacuum gap perpendicular to the surface normal of at

least 20 Å to ensure negligible interactions between repeated images in neighboring cells. All the inputs and calculations were generated and performed within the Atomic Simulation Environment version 3.19.0 [47].

C. Calculated properties

In this section, we will describe how we have computed the different properties used in our comparison of the different density functionals. In all cases, total energies and structures are consistently used, i.e., energies are always taken from optimized geometries at the same level of theory.

1. Bulk cohesive energy

The bulk cohesive energy is calculated as the energy difference per atom:

$$E_{\text{coh}} = E_{\text{at}} - \frac{E_{\text{bulk}}}{N}, \quad (4)$$

where E_{at} is the total energy of an isolated atom in a $12 \text{ \AA} \times 13 \text{ \AA} \times 14 \text{ \AA}$ cell, E_{bulk} is the total energy of the bulk crystal, and N is the number of atoms in the bulk crystal. With this definition, the stronger the chemical bond in bulk is, the larger the positive value of the cohesive energy E_{coh} . One known problem in the calculation of cohesive energies is the difficulty for local and semilocal density functionals describing atomic energies. Atoms are typically open-shell systems, which are often very difficult to converge within the used computational setup. To circumvent this problem, we also compare energy differences and evaluate the capability of each functional to predict different crystal structures of the same material accurately. For Ni, the cohesive energy for the fcc phase was compared against the cohesive energy of the more rarely occurring bcc phase.

2. Surface energy

We calculated the surface energies for the various generated slab models according to

$$E_{\text{surf}} = \frac{E_{\text{slab}} - nE_{\text{bulk}}^{\text{fcc}}}{2A}, \quad (5)$$

where E_{slab} is the total energy of the slab model representing the low Miller index surface structure of interest within the supercell approach, $E_{\text{bulk}}^{\text{fcc}}$ is the total energy of the fcc Ni bulk in units of eV/atom, and n is the number of atoms in the slab model, and A is the area of the slab model. Since the slab model contains two equivalent surfaces, the considered surface area is doubled [factor 2 in Eq. (5)].

3. Work function

The work function is defined as the energy needed to extract one electron from the Fermi level of a material to vacuum. In the supercell approach, the absolute value of the vacuum energy is not known, as the electrostatic potential by definition is averaged to be zero in the plane wave formalism of DFT. In this work, we used the macroscopic average approach, where the difference in the planar averaged electrostatic potential in the middle of the vacuum gap, V_{vac} , and in the middle of the slab, V_{slab} , are used to define a potential

offset, $\Delta V = V_{\text{vac}} - V_{\text{slab}}$. This quantity is then referenced to the bulk potential, $V_{\text{bulk}}^{\text{macro}}$, and allows using the Fermi energy $\varepsilon_{\text{bulk}}^F$ from a bulk calculation. By doing that, the calculated work function does not suffer from quantum size effects [48,49]. The work function is then:

$$\phi = \Delta V + V_{\text{bulk}}^{\text{macro}} - \varepsilon_{\text{bulk}}^F. \quad (6)$$

4. Wulff construction /shape

To quantify the effect that the choice of functional will have on predicted nanoparticle shapes, we have determined the expected nanoparticle shapes using the Wulff construction scheme [50] as implemented in the Python library Wulffpack version 0.3 [51]. The input in this scheme is the calculated surface energies at various levels of theory.

IV. RESULTS AND DISCUSSION

In this section, we discuss the impact that the choice of exchange-correlation energy description has on the investigated properties. We start with the results for the bulk structures and continue with results for the low Miller index Ni surfaces and end with the functional effect of the predicted nanoparticle shapes. After that, we turn to an analysis based on the reduced density gradient where we rationalize the results in order to extend and generalize our understandings.

A. Bulk metals: fcc and bcc Ni

We investigate how different density functionals treat metallic fcc and bcc Ni when it comes to structural and energetic properties. Before presenting our results, we first comment on the distribution of computed reduced density gradients s in the two bulk systems. The calculated s values at the PBE level of theory are given in the histogram plot in Fig. 3(a) for both fcc and bcc Ni. As expected, only low s values (close to 0) are found for these metallic compounds. Given the fact that the exchange enhancement factor $F_x(s)$ approaches one as s goes to 0 in all functionals, we expect that they should all behave similarly for many of the bulk properties [cf., Fig. 1(a)]. So, let us see if this is the case.

It stands clear that one property that will differ is the cohesive energy (see Sec. III C1) because it involves the total energy of the atom, which shows higher s values [cf., Fig. 1(d)]. Cohesive energies E_{coh} for fcc Ni computed with the 11 different density functionals are given in Table SI of the Supplemental Material [52], which also includes Refs. [53–58]. The error calculated versus the experimental result extrapolated to 0 K (4.48 eV/atom) are shown in Fig. 3(b). As expected, we see large differences in calculated cohesive energies, with errors as large as 30% for some functionals. However, if we instead look at energy differences for the different bulk phases of Ni, all functionals predict similar values [cf., Table SI and Fig. 3(c)]. This supports the hypothesis that the problem lies in the computation of the total energy of the Ni atom. Here, we further note that all functionals correctly predict that fcc is more stable than the bcc phase of Ni.

Let us have a closer look at the results and start with the standard semilocal functionals without any explicit or *a posteriori* treatment of dispersion. In Sec. II, we divided the

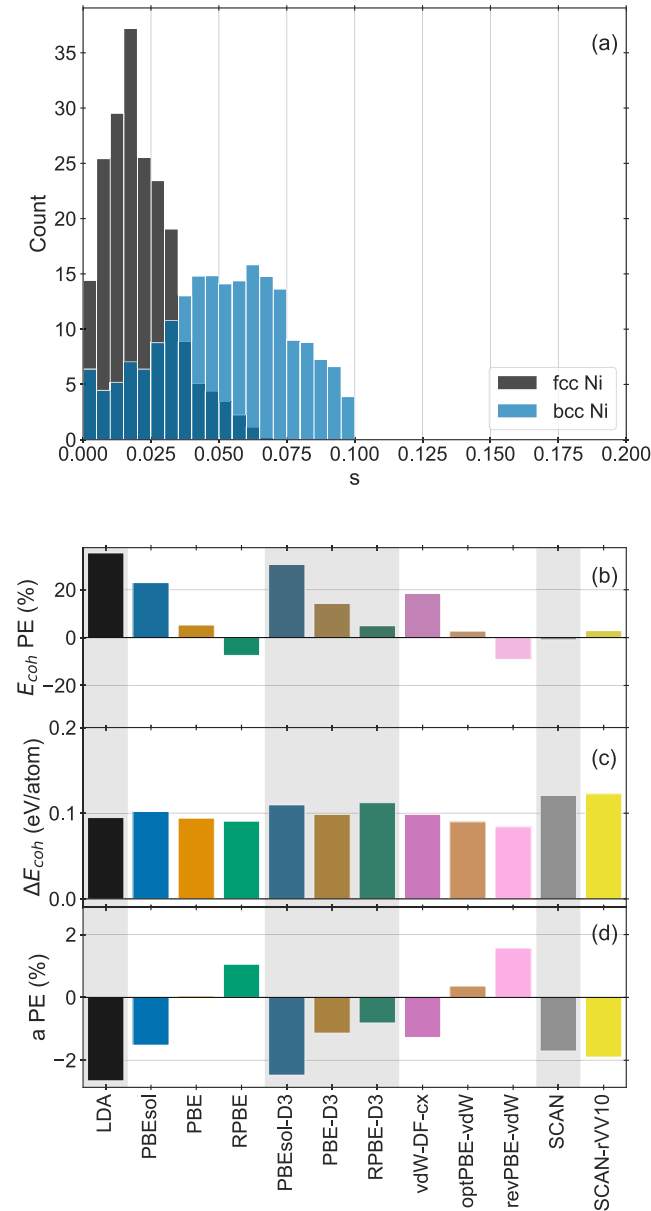


FIG. 3. (a) s values found in fcc and bcc bulk Ni, respectively. (b) fcc bulk Ni cohesive energies percentage error (PE), (c) fcc-bcc energy difference $\Delta E_{\text{coh}} = E_{\text{coh}}^{\text{fcc}} - E_{\text{coh}}^{\text{bcc}}$, and (d) the error in estimated fcc bulk Ni lattice parameter with respect to experiment.

different functionals into subsets relative to the PBE density functional. We note that the functional that has been made to improve on molecular properties, i.e., the RPBE functional, underestimates the E_{coh} value while the functional with a focus on improved bulk properties (i.e., PBEsol) strongly overestimates E_{coh} when compared to the value obtained at the PBE level of theory. Based on the discussion in Sec. II, and comparing the $F_x(s)$ for PBE, RPBE, and PBEsol shown in Fig. 1, we can now trace a trend in cohesive energy to the steepness of $F_x(s)$ as s goes from 0 to larger values.

Adding an *a posteriori* dispersion correction via the Grimme D3 correction results in a larger E_{coh} compared to the parent method without dispersion due to a stabilization

of the bulk phase, since the atom energy remains the same. Hence, for all semilocal density functionals, the inclusion of an *a posteriori* dispersion correction worsens the E_{coh} in comparison to the experimental value, except for RPBE. The functionals with a self-consistent treatment of the nonlocal correlation follow the very same trend as the standard semilocal functional, i.e., the steepness of $F_x(s)$ is strongly correlated to the relative differences found in computed E_{coh} values.

The meta-GGA functional, SCAN, performs very well for the cohesive energy with the smallest error compared to experiments of all tested functionals. The inclusion of self-consistent dispersion in the form of the rVV10 model makes it slightly worse.

The results presented here are in line with what has been found previously in the literature. Jana *et al.* [59] compared bulk properties using two semilocal GGA functionals (PBE and PBEsol) and many meta-GGA functionals for various bulk systems, including SCAN. They observed the same trend for GGA functionals that PBE and PBEsol overestimate the Ni cohesive energy. However, for the meta-GGA SCAN density functional, they computed a much higher Ni cohesive energy (5.25 eV/atom compared to our value of 4.44 eV/atom). We do not know the reason for this discrepancy at this point, but we note that it is occasionally hard to reach electronic convergence in the SCAN calculations. For this functional, our results are in better agreement with those of Zhang *et al.* [60], who compared six different functionals (PBE, PBEsol, SCAN, M06-L, and HSE06) for 64 bulk solids and found that both PBE and SCAN have a mean error of only -0.08% . Furthermore, Tran, Stelzl, and Blaha [61] found in their study of bulk solids that data obtained using a meta-GGA functional are more accurate than data obtained using semilocal GGA, and thereby concluded that the inclusion of the electronic kinetic energy density is an essential ingredient to reach chemical accuracy for energy-related properties.

When it comes to structural properties, we compare the calculated lattice constants with the experimentally measured value extrapolated to 0 K. The computed data is given in Table SI, and the calculated percentage error with respect to the experimental value is shown in Fig. 3(d). Here we note that the errors are much smaller than for cohesive energies. This is consistent with the hypothesis that the poor prediction of cohesive energies seen for many of the functionals primarily stems from an inadequate description of the atom. As for the cohesive energy, we see a strong correlation between the steepness of $F_x(s)$ and the computed lattice constant. Among the semilocal functionals, PBE reproduces the experimentally measured lattice constant. Introducing an *a posteriori* dispersion correction leads to a contraction of the solids compared to the parent method without the correction. None of the tested functionals that belong to the Rutgers-Chalmers family are as good as PBE when it comes to the lattice parameter. However, optPBE-vdW comes close. For the meta-GGA functional SCAN, we note that it does not perform as well as for the cohesive energy, and the inclusion of self-consistent dispersion based on the rVV10 model again makes the performance slightly worse. In Table SI we additionally provide the computed lattice constants for the bcc phase of Ni, which follows the same trend as found for the fcc phase. For the bcc phase, which is a metastable phase for Ni, there is, however,

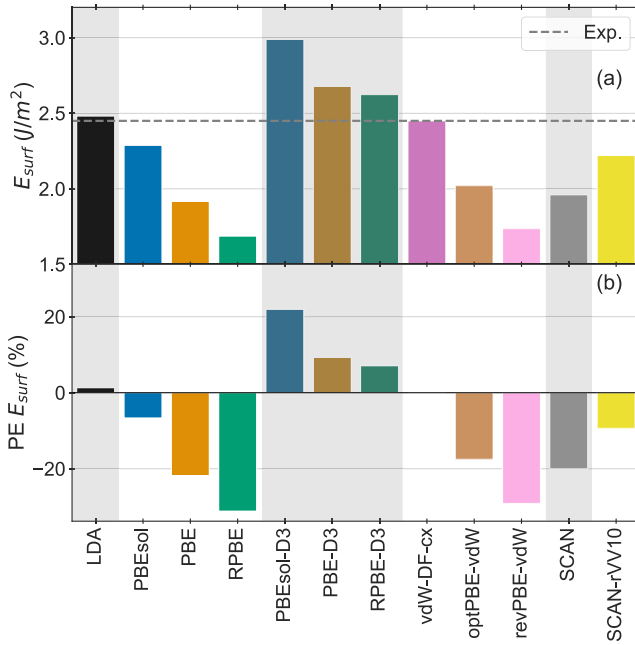


FIG. 4. (a) shows the computed surface energy of Ni(111) and (b) the percentage error for the computed surface energy with respect to experiment for LDA, various semilocal GGA functionals, and the meta-GGA functional SCAN with and without accounting for dispersion interactions.

a larger spread when it comes to the experimentally measured values [56–58]. This makes the comparison to experiments hard in this case. We address this issue later in Sec. IV F.

For the structural properties, our results for the fcc phase agree to what has been reported in the literature. Zhang *et al.* [60] found similar results for the lattice parameter of Ni, with PBE being the most accurate among the investigated functionals. PBEsol and SCAN were found to underestimate the lattice parameters. Similar findings have also been seen by Jana *et al.* [59].

B. Ni metal surfaces

1. Surface energy

We start with the absolute values of the surface energies calculated for Ni(111), as shown in Fig. 4(a) and given in Table SII in the Supplemental Material [52], which also includes experimental results from Refs. [62,63]. We first note that despite the largely overestimated cohesive energy, the LDA functional only slightly overestimates the surface energy. All tested GGA functionals underestimate the surface energy. The PBEsol functional, which is the semilocal GGA functional constructed to be accurate for the condensed phase, is here the GGA functional that performs best, however worse than LDA. PBE underestimates the absolute value by more than 10%, and the more “molecularly tuned” functional (RPBE) severely underestimates the surface energy, with an error in the order of 30%.

The inclusion of *a posteriori* dispersion corrections using the D3-Grimme approach always increases the surface en-

ergy, making all functionals overestimating the absolute value with around 20% for PBEsol-D3 and 10% for PBE-D3 and RPBE-D3.

For the vdW family of functionals, we again see the same trend as expected concerning the behavior of $F_x(s)$, cf., Fig. 4(a). Here, vdW-DF-cx is the most accurate among the investigated vdW-DF functionals, with a percentage error of -0.02% . The functional optPBE-vdW shows larger error (-17.51%), cf., Table SII, whereas revPBE-vdW underestimates the surface energy by about 30%. The meta-GGA functional SCAN performs similarly as the PBE functional, which means that the absolute value for the surface energy is underestimated by about 20%. Here, accounting for dispersion through the rVV10 model improves the results, however, still worse than the semilocal PBEsol functional (-9.36% vs -6.63% , respectively), cf., Fig. 4(b). These results are in line with the ones reported by Patra *et al.* [64], who found that SCAN-rVV10 provides a mean absolute percentage error (MAPE) for a series of metal fcc surfaces of 5%. For the semilocal functionals accounting for dispersion, Hyldgaard and Jiao have previously reported that vdW-DF-cx was the most accurate functional when comparing calculated properties for a series of transition metals with a MAPE of 7% [65]. Avelar *et al.* [66] tested four different vdW-DF functionals and found that the vdW-DF-C09_x functional had the smallest MPE for a series of transition metals surfaces (MPE = -10.2%). For Ni(111), vdW-DF-C09_x underestimated the surface energy by 5.31% [65], which is not surprising since the vdW-DF-C09_x is a very similar functional when compared to vdW-DF-cx. However, the different treatment in the exchange energy for the latter makes it better when it comes to surface energies. Table SII also summarizes the data obtained for the Ni(110) and Ni(100) surfaces. Even if the surface energy is off by 20–30% on the absolute scale, all functionals still predict the (110) and (100) surfaces to be less stable than the (111) surface, which is in accordance with experimental data. We observe that the computed surface energies for (110) and (100) follow a similar dependence on the exchange enhancement factor as the (111) surface.

2. Ni(111) work function

The work function is a property that depends strongly on the electron density and is, therefore, an important property to consider when evaluating the accuracy of different density functionals. We start with the Ni(111) surface, for which the results are given in Fig. 5(a), and Table SII. In the latter, we additionally report the Ni(100) and Ni(110) results. However, as the computed trend is similar, we will concentrate the discussion on the work function computed for the Ni(111).

For LDA and semilocal GGA functionals without dispersion corrections, we find that the functionals behave similarly as for the surface energies, i.e., the steeper $F_x(s)$ is for small s , the lower the work function, which in turn leads to that while PBEsol slightly underestimates the target value, the computed values using the PBE and RPBE density functionals underestimate even more.

For the same atomic configuration, *a posteriori* dispersion corrections using the Grimme D3 method do not affect the

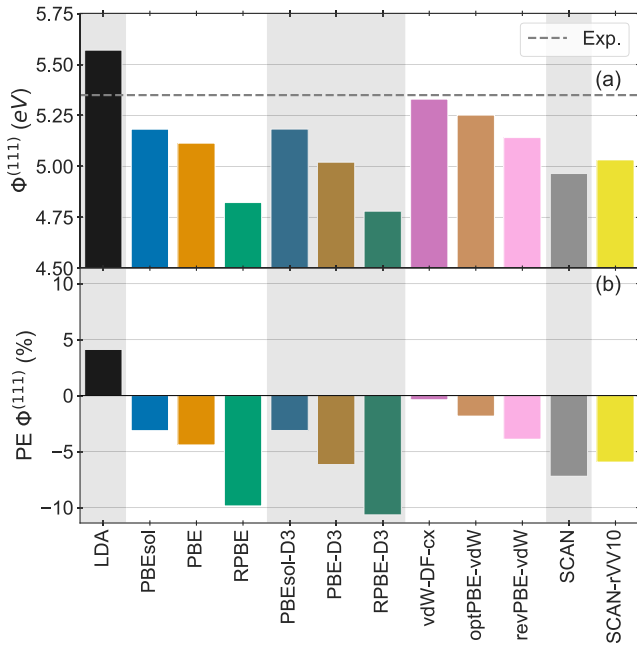


FIG. 5. (a) Computed work functions for Ni(111) and (b) the percentage error for the computed surface energy concerning experiment for LDA and various semilocal GGA functionals and the meta-GGA functional SCAN with and without accounting for dispersion interactions.

electronic structure and therefore lead to the same results when compared to the ones obtained using its parent GGA density functional. However the inclusion of the Grimme D3 model tends to shrink the bulk lattice upon geometry optimization. From the data reported in Fig. 5(a), we find that the effect of this contraction on the computed work function is very small.

Similarly, the vdW-DF functionals behave as they did for the surface energies. We find that all tested functionals perform well with an absolute percentage error below 5%, and vdW-DF-cx is the most accurate among the tested functionals with an error of -0.37% compared to the experimental value for the Ni(111) surface. Concerning the meta-GGA functional SCAN, the calculated work function is similar to the PBE results, underestimating the experimental results by about 7%. As for the semilocal functionals, adding a dispersion correction, here in the form of the rVV10 model, slightly improves the calculated work function, with an error of -5.94% [cf., Fig. 5(b)]. Still, the vdW-DF functionals seem on average to be more accurate in predicting the work function.

Patra *et al.* [64] calculated the mean work function for eight transition metals and reported similar MAPE for PBEsol, SCAN, and the SCAN-rVV10 functionals. Hyldgaard and Jiao [65] additionally reported results for vdW-DF-cx using the same metals as Patra *et al.* and found in agreement with our results that the inclusion of dispersion corrections self-consistently through the vdW-DF approach improves the predictive power of work functions for transition metals.

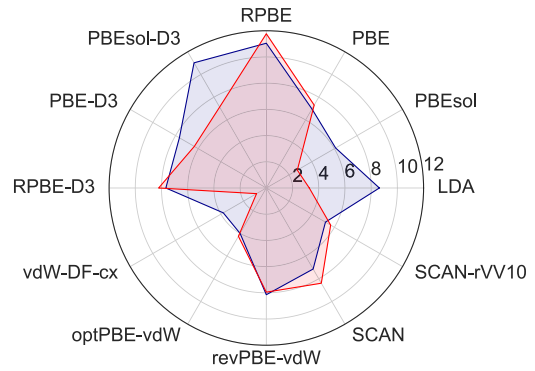


FIG. 6. Mean absolute percentage error chart (in %) for Ni fcc and Ni(111) surface. (blue) Properties that account for the atom energy and (red) properties that do not account for atom energy.

C. Summary of quantitative results

The computed MAPE for all presented results are summarized in the radar chart seen in Fig. 6. Notably, PBE comes out very well, which explains why this functional is a popular choice for applications in materials science. PBEsol cohesive energies are known to be inaccurate, because of the poor performance for the atom. If we remove this property, as has been done in the red radar chart also presented in Fig. 6, the performance of the PBEsol functional comes out much better, and the MAPE goes from 6.11% to 2.73%. The effect of adding *a posteriori* Grimme D3 dispersion correction to these functionals does not always lead to an improved description and will depend on the starting point, as seen in Fig. 6. For PBEsol, the error becomes larger, while the PBE MAPE is roughly the same. For RPBE, however, which shows a large error without dispersion corrections, the results are significantly improved upon the inclusion of the Grimme D3 correction. The reason for this behavior is that the Grimme D3 term is always additive in terms of energy and at the same time leads to an attractive interaction. This means that a functional that without dispersion correction underestimates energetic properties and overestimates structural properties will benefit from the *a posteriori* correction, while the opposite holds for vice versa. Similar observations have been seen for crystalline hydrates [43]. However, it is unclear if this conclusion can be generalized to all *a posteriori* methods. DFT-D3 was originally designed for the main group elements, while some other methods, such as uMDB [19] and XDM [20], have been developed for the condensed phase and would need to be assessed separately.

For the vdW-DF family of functionals, we note that vdW-DF-cx comes out as the best if all properties are compared (MAPE = 3.79%, Fig. 6 blue) and when removing the reference to the atom in the form of the cohesive energy (MAPE = 0.86%, Fig. 6 red). The meta-GGA functional SCAN combined with the rVV10 model for dispersion interactions has a similar performance to the GGAs, with MAPE of 5.21% and 5.67% in case of the inclusion of the atomic energies, respectively (cf., Fig. 6).

The conclusion from these results is that dispersion corrections are vital to improve the accuracy of semilocal DFT calculations, and in that way, increases the predictive power in

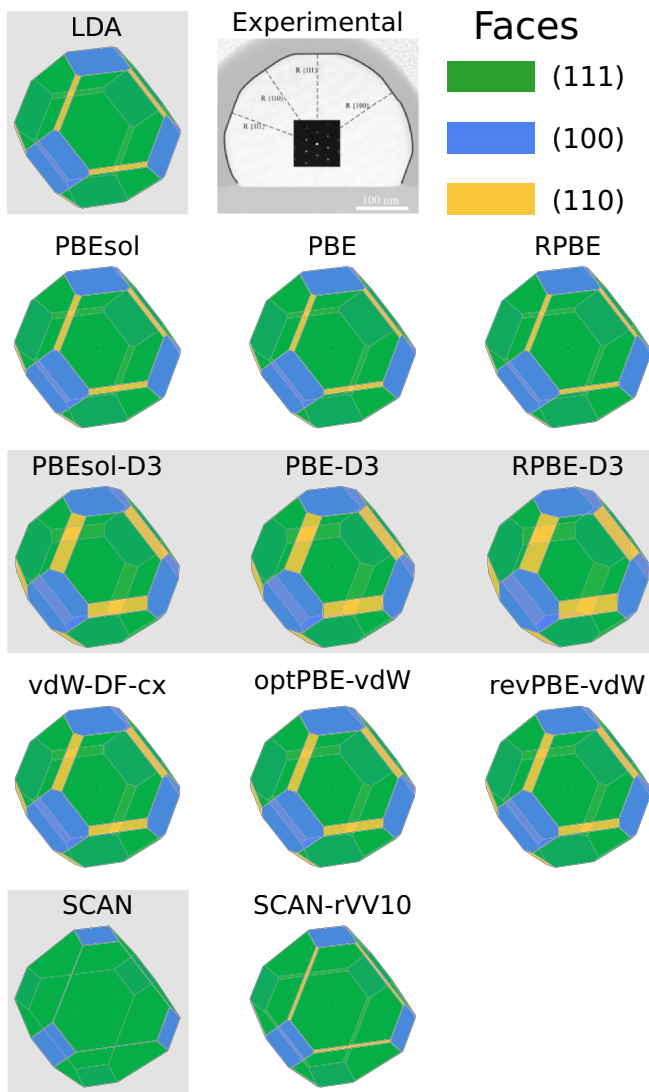


FIG. 7. Predicted nanoparticle shapes for LDA and various semilocal GGA functionals and meta-GGA functional SCAN with and without accounting for dispersion interactions. The experimental result is taken from Ref. [67]. Reprinted with permission. Copyrights® Elsevier 2020.

materials science. However, when including these corrections, care must be taken when choosing a matching exchange description.

D. Qualitative analysis: Predicting the shape of Ni nanoparticles

The crystal shape of nanoparticles can be predicted using the Wulff construction scheme [50], which effectively takes into account the relative surface energy for different facets. As such, this measure does not rely on the quantitative accuracy concerning absolute values of the surface energies but rather on the ratio between them. With the calculated surface energies of the low Miller index surfaces reported in Table SII, we have constructed Wulff shapes for Ni with data from all considered functionals, and the results are given in Fig. 7. As discussed in previous sections, the energies of the various surface facets are strongly correlated. We could, therefore,

expect that all functionals give rise to similar Wulff shapes. However, as seen in Fig. 7, subtle differences in relative energies of the different facets lead to notable variations in the particle shape, seen mainly in the proportion of exposed (110) surface, cf., Fig. 7.

For all evaluated GGA functionals (cf., Fig. 7 second row), the estimated particle shape displays significantly less (110) surface compared to the shape predicted using the D3 corrections (cf., Fig. 7 third row). The vdW-DF functionals predict very similar shapes, with the fraction of exposed (110) surface area between the GGA and GGA-D3 predictions. Compared to the GGAs, the meta-GGA functionals SCAN and SCAN-rVV10 predict smaller (or even nonexisting) fraction of exposed (110) surface area (cf., Fig. 7 last row gray background, and Fig. 7 last row white background). We note that applying a dispersion correction using the self-consistent rVV10 model has minimal effect on the predicted shape for the SCAN functional.

Comparing the theoretical predictions for the Ni particle shape with experiments, cf., Fig. 7, we note that both have the (111) surface as the dominant facet, followed by the (100) and (110) facets. It is worth mentioning that at low oxygen pressures, there are substantial areas of exposed (110) facets [67], which is in agreement with the theoretical results obtained using the semilocal functional accounting for dispersion interactions.

E. Rationalizing the results in terms of the reduced density gradient

In the previous sections, we have reported computed properties obtained with different levels of theory for Ni in three different cases: bulk, surface, and atom. We will now look at the results a little bit closer and rationalize them in terms of a general feature, namely the reduced density gradient s . Based on the results obtained in the quantitative analysis above, we have noted that the accuracy is correlated to the initial steepness of $F_x(s)$, for $0 < s \lesssim 2$. Therefore, our hypothesis is that it should be possible to find a single number s_0 to represent the different distributions of s [cf., e.g., Figs. 1(b)–1(d)] that optimizes the correlation of $F_x(s_0)$ and computed properties. To find s_0 , we screened 1000 evenly spaced s values between 0 and 5 and calculated $F_x(s)$ for each functional. Thereafter, we used linear regression to find the optimal correlation with respect to each considered property. Since a linear regression requires at least three different values of $F_x(s)$, we divided the functionals into classes following the discussion in Sec. II. The classes are (i) GGA: PBEsol, PBE, and RPBE, (ii) GGA-D3: PBEsol-D3, PBE-D3, and RPBE-D3, and (iii) vdW-DF: vdW-DF-cx, optPBE-vdW, and revPBE-vdW. Note, with this procedure there is one s_0 for each combination of functional class and property. The optimal s_0 values for each property and functional class are given in Table I.

Let us first look at bulk properties and the surface energy for the (111) facet. For each optimal value s_0 we obtain a correlation plot between the $F_x(s_0)$ and a certain property, as shown in Fig. 8. For comparison, the experimental results are also given in the figure (horizontal dashed lines). We note that the regression obtained for GGA and vdW-DF classes cross the horizontal experimental line without having to extrapolate

TABLE I. s_0 values (see definition in the text) for each investigated property and each class of functional.

Functional class	Property						
	$E_{\text{coh}}^{\text{fcc}}$	$E_{\text{coh}}^{\text{bcc}}$	$a_{\text{latt}}^{\text{fcc}}$	$a_{\text{latt}}^{\text{bcc}}$	$E_{\text{surf}}^{(111)}$	$E_{\text{surf}}^{(100)}$	$E_{\text{surf}}^{(110)}$
GGA	1.61	1.62	1.51	1.48	1.48	1.48	1.48
GGA-D3	1.41	1.45	0.89	0.92	0.76	1.02	0.97
vdW-DF	1.34	1.35	1.32	1.27	1.11	1.10	1.11

it beyond the calculated values, while the regression for GGA-D3 does not. We reach a similar conclusion for the bulk properties, here in the form of cohesive energy and lattice parameters, as for surface energies, see Fig. 8(c). Interestingly, our regression models clearly expose the procrustean dilemma often found in density functional development [68], here seen in the fact that the different properties do not cross the experimental reference at the same $F_x(s_0)$ value. This implies that no semilocal GGA would be capable of an accurate description of both total energy and structural properties.

F. Extrapolated bcc Ni lattice constant, cohesive energy, and Wulff shape

In the previous section, we showed that there is an optimal s value for each functional class that results in a strong correlation between the obtained exchange enhancement factor and each computed property. We further elaborate on this observation and show that this correlation can be used to predict properties that are difficult to measure experimentally. A procedure to estimate the bcc Ni lattice constant is shown in Fig. 9, which from experiments is poorly determined due to problems of stabilizing Ni in this metastable phase. The

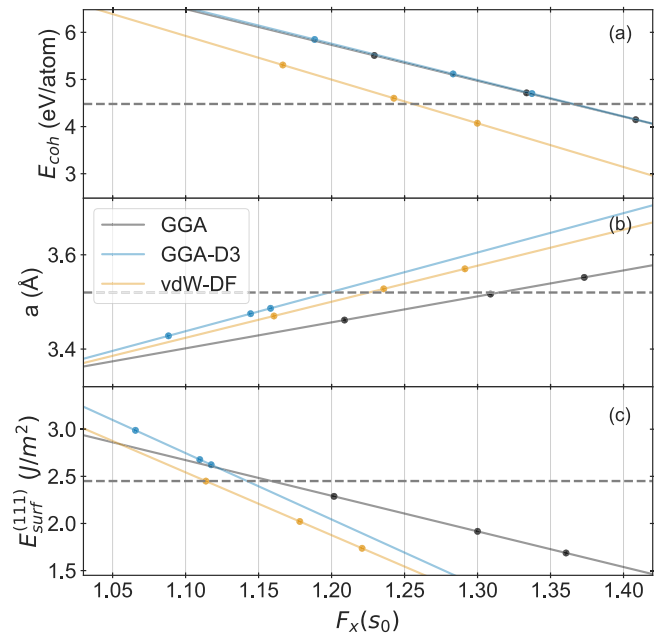


FIG. 8. Correlation plot between bulk properties and optimal F_x for (a) bulk cohesive energy, (b) lattice parameter, and (c) Ni(111) surface energy. The dashed lines represent the experimental values.

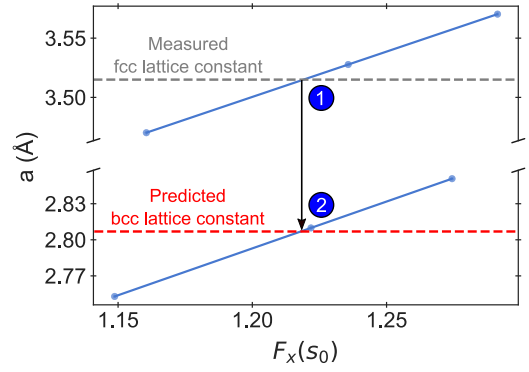


FIG. 9. Schematic representation for the predicted Ni bcc lattice constant. The same procedure is applied for Ni(100) and Ni(110) surface energies.

procedure is as follows: (i) find $F_x(s_0)$ that crosses the experimental value for the fcc lattice constant (denoted 1 in Fig. 9), (ii) draw a vertical line through this point, and (iii) read out the predicted experimental value for the bcc lattice constant at the same $F_x(s_0)$ value (depicted 2 in Fig. 9).

The predicted lattice parameter for the Ni bcc lattice constant obtained in this way becomes 2.810, 2.797, and 2.805 Å for GGA, GGA-D3, and vdW-DF, respectively (Table II). The predicted values for the GGA and vdW-DF classes are in good agreement with the experimental data measured on nano-sized bcc Ni particles ranging from 2.82–2.90 Å [56,57,61]. Applying the same scheme for predicting the bcc cohesive energy, i.e., using the correct experimental measure for fcc to predict the experimental cohesive energy for bcc, we obtain a difference between the fcc experimental and the bcc predicted values of 0.10 eV/atom for the GGA and the vdW-DF class of functionals, while the Grimme corrected functionals give 0.00 eV/atom. Clearly, the latter is at variance with the experimental observation that the bcc structure is difficult to stabilize and suggest that adding *a posteriori* corrections disturb the accuracy and predictive power of our procedure.

With the same prediction procedure as depicted in Fig. 9, we can obtain extrapolated Ni(100) and (110) surface energies, for which no experimental data exist. The predicted surface energies are given in Table II. While the GGA and vdW-DF classes predict that $E_{\text{surf}}^{(100)} < E_{\text{surf}}^{(110)}$ (see Table II and Fig. 10), the Grimme corrected GGA functionals yield the opposite trend. Also, the absolute values obtained with the D3-corrected functionals are larger, while the other two functionals yield similar results (within 0.06 J/m²).

TABLE II. Predicted experimental values for the bulk and surface properties of Ni.

Functional class	Predicted experimental values			
	$E_{\text{coh}}^{\text{bcc}}$	$a_{\text{latt}}^{\text{bcc}}$	$E_{\text{surf}}^{(100)}$	$E_{\text{surf}}^{(110)}$
GGA	4.40	2.810	2.82	2.92
GGA-D3	4.48	2.797	3.17	3.18
vdW-DF	4.40	2.805	2.76	2.86

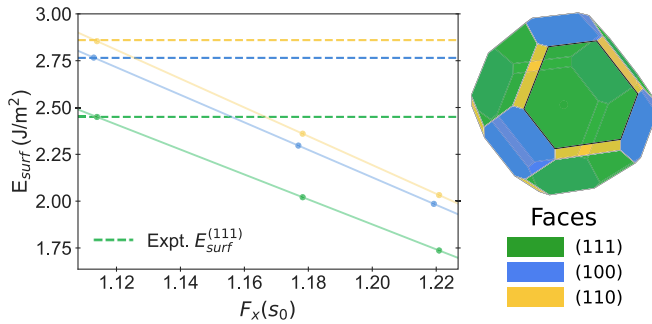


FIG. 10. Predicted experimental Wulff shape using surface energies obtained through the linear regression method. In the figure, data from the vdW-DF class of density functionals are shown.

With these results, we can build a Wulff shape as done in Sec. IV D but now with extrapolated surface energies. In Fig. 10 we use the data obtained for the vdW-DF class as an example. We note that the shape is qualitatively the same by comparing the predicted experimental Wulff shape to the ones we obtained for the individual functionals (cf., Fig. 7).

With these examples, we demonstrated standard features of three functional classes employed in materials science. By choosing a set of functionals that describes properties of interest with satisfactory accuracy, we can obtain an understanding of their limitations by analyzing a common feature, the reduced density gradient. We can now extend the same methodology for even more complex systems, with a wider reduced density gradient distribution, such as bulk and surface alloys, and multicomponent nanoparticles.

V. CONCLUSIONS

We have evaluated the performance of different semilocal GGA type of functionals with and without dispersion corrections in describing bulk and surface properties of Ni to provide an understanding of how different components in a modern density functional affect their accuracy. To generalize the obtained understandings, we additionally rationalize the results in terms of the reduced density gradient s and the exchange enhancement factor $F_x(s)$. In addition, we also make comparisons against the meta-GGA functional SCAN and SCAN-rVV10, which claims to solve many of the deficiencies found in standard semilocal density functional theory.

We find that for the semilocal functionals, all examined properties show a strong correlation with the steepness of the exchange enhancement factor, $F_x(s)$, as s , the reduced density gradient, goes from 0 to larger values. With increasing steepness [in the current work characterized by the $F_x(s_0)$], we find the following effect on the various properties using semilocal functionals without dispersion correction:

- (i) Cohesive energies decrease.
- (ii) Lattice parameters increase.
- (iii) Surface energies decrease.

We observe the same trend after applying the DFT-D3 dispersion correction method but with systematic shifts towards

larger cohesive energies, smaller lattice constants, and larger surface energies. Within the family of vdW-DF density functionals, which contain a self-consistent treatment of the non-local correlation, the strong correlation between the computed properties and $F_x(s_0)$ remains, but we see systematic shifts towards smaller cohesive energies, larger lattice constants, while the surface energies were less affected when compared to the semilocal functionals without dispersion correction.

In comparison to experiments, we find that the most accurate functionals are (with percentage error compared to experiment in parenthesis):

- (i) SCAN, for cohesive energy of fcc Ni (−0.89%).
- (ii) PBE, for lattice parameter of fcc Ni (0.05%).
- (iii) vdW-DF-cx, for surface energy of the Ni(111) surface (−0.02%).
- (iv) vdW-DF-cx, for work function of the Ni(111) surface (−0.37%).

The meta-GGA functional, SCAN, without self-consistent dispersion correction, slightly improves the calculated properties with an average percentage error of 7.14%. Moreover, adding dispersion interactions, the average percentage error lowers to 5.21%, showing the importance of dispersion interactions in DFT.

In this work, we have evaluated these functionals qualitatively and quantitatively. The best overall description is given by vdW-DF-cx, followed by optPBE-vdW and SCAN-rVV10, in which they have an average percentage error of 3.79%, 4.00%, and 5.21%, respectively (see Fig. 6). We qualitatively compared computed predicted particle shapes using Wulff constructions. We note that while quantitative errors can be very large, the relative errors are effectively canceled, resulting in similar particle shapes.

To generalize the obtained understanding, all obtained results are rationalized using the reduced density gradient s as a measure. We have found that there is a correlation between surface and bulk properties and the steepness in the functional exchange enhancement factor upon increasing s values. We have found it convenient to use a value of s_0 that optimizes the correlation between $F_x(s)$ and the property of interest. We further propose and validate a scheme to predict experimentally unknown properties, here exemplified by the Ni bcc lattice constant, as well as Ni(100) and Ni(110) surface energies. We believe that this correlation can be generalized for more complex materials and broader reduced density gradient distributions.

ACKNOWLEDGMENTS

This work is supported by the Swedish Research Council (VR) (PB). Funding from the National Strategic e-Science program eSSSENCE is greatly acknowledged. The simulations were performed on resources provided by the Swedish National Infrastructure for Computing (SNIC) at UPPMAX, HPC2N, and NSC.

- [1] K. Duanmu and D. G. Truhlar, Validation of density functionals for adsorption energies on transition metal surfaces, *J. Chem. Theory Comput.* **13**, 835 (2017).
- [2] N. Mardirossian and M. Head-Gordon, Thirty years of density functional theory in computational chemistry: an overview and extensive assessment of 200 density functionals, *Mol. Phys.* **115**, 2315 (2017).
- [3] J. K. Norskov, F. Abild-Pedersen, F. Studt, and T. Bligaard, Density functional theory in surface chemistry and catalysis, *Proc. Natl. Acad. Sci.* **108**, 937 (2011).
- [4] R. Ferrando, J. Jellinek, and R. L. Johnston, Nanoalloys: from theory to applications of alloy clusters and nanoparticles, *Chem. Rev.* **108**, 845 (2008).
- [5] L. Liu and A. Corma, Metal catalysts for heterogeneous catalysis: From single atoms to nanoclusters and nanoparticles, *Chem. Rev.* **118**, 4981 (2018).
- [6] R. A. Boto, J. Contreras-García, J. Tierny, and J.-P. Piquemal, Interpretation of the reduced density gradient, *Mol. Phys.* **114**, 1406 (2015).
- [7] A. Zupan, K. Burke, M. Ernzerhof, and J. P. Perdew, Distributions and averages of electron density parameters: Explaining the effects of gradient corrections, *J. Chem. Phys.* **106**, 10184 (1997).
- [8] P. Hohenberg and W. Kohn, Inhomogeneous electron gas, *Phys. Rev.* **136**, B864 (1964).
- [9] J. P. Perdew, K. Burke, and M. Ernzerhof, Generalized Gradient Approximation Made Simple, *Phys. Rev. Lett.* **77**, 3865 (1996).
- [10] J. P. Perdew, K. Burke, and M. Ernzerhof, Generalized Gradient Approximation Made Simple [Phys. Rev. Lett. 77, 3865 (1996)], *Phys. Rev. Lett.* **78**, 1396 (1997).
- [11] J. P. Perdew, A. Ruzsinszky, G. I. Csonka, O. A. Vydrov, G. E. Scuseria, L. A. Constantin, X. Zhou, and K. Burke, Restoring the Density-Gradient Expansion for Exchange in Solids and Surfaces, *Phys. Rev. Lett.* **100**, 136406 (2008).
- [12] B. Hammer, L. B. Hansen, and J. K. Nørskov, Improved adsorption energetics within density-functional theory using revised perdue-burke-ernzerhof functionals, *Phys. Rev. B* **59**, 7413 (1999).
- [13] J. Tao, J. P. Perdew, V. N. Staroverov, and G. E. Scuseria, Climbing the Density Functional Ladder: Nonempirical Meta-Generalized Gradient Approximation Designed for Molecules and Solids, *Phys. Rev. Lett.* **91**, 146401 (2003).
- [14] J. Sun, A. Ruzsinszky, and J. Perdew, Strongly Constrained and Appropriately Normed Semilocal Density Functional, *Phys. Rev. Lett.* **115**, 036402 (2015).
- [15] S. Grimme, Accurate description of van der waals complexes by density functional theory including empirical corrections, *J. Comput. Chem.* **25**, 1463 (2004).
- [16] S. Grimme, Semiempirical GGA-type density functional constructed with a long-range dispersion correction, *J. Comput. Chem.* **27**, 1787 (2006).
- [17] S. Grimme, J. Antony, S. Ehrlich, and H. Krieg, A consistent and accurate *ab initio* parametrization of density functional dispersion correction (DFT-D) for the 94 elements h-pu, *J. Chem. Phys.* **132**, 154104 (2010).
- [18] A. Tkatchenko and M. Scheffler, Accurate Molecular Van Der Waals Interactions from Ground-State Electron Density and Free-Atom Reference Data, *Phys. Rev. Lett.* **102**, 073005 (2009).
- [19] M. Kim, W. J. Kim, T. Gould, E. K. Lee, S. Lebègue, and H. Kim, uMBD: A materials-ready dispersion correction that uniformly treats metallic, ionic, and van der waals bonding, *J. Am. Chem. Soc.* **142**, 2346 (2020).
- [20] M. S. Christian, A. O. de-la Roza, and E. R. Johnson, Adsorption of graphene to metal (111) surfaces using the exchange-hole dipole moment model, *Carbon* **124**, 531 (2017).
- [21] H. Rydberg, B. I. Lundqvist, D. C. Langreth, and M. Dion, Tractable nonlocal correlation density functionals for flat surfaces and slabs, *Phys. Rev. B* **62**, 6997 (2000).
- [22] R. Sabatini, T. Gorni, and S. de Gironcoli, Nonlocal van der waals density functional made simple and efficient, *Phys. Rev. B* **87**, 041108 (2013).
- [23] N. Ferri, R. A. DiStasio, A. Ambrosetti, R. Car, and A. Tkatchenko, Electronic Properties of Molecules and Surfaces with a Self-Consistent Interatomic Van Der Waals Density Functional, *Phys. Rev. Lett.* **114**, 176802 (2015).
- [24] D. C. Langreth and S. Vosko, Response functions and nonlocal approximations, *Advances in Quantum Chemistry* (Elsevier, San Diego, California, 1990), pp. 175–199.
- [25] J. P. Perdew, Jacob's ladder of density functional approximations for the exchange-correlation energy, in *Density Functional Theory and its Application to Materials*, edited by V. Van Doren, C. Van Alsenoy, and P. Geerlings, AIP, Conf. Proc. No. 557 (AIP, Antwerp, Belgium, 2001), p. 1.
- [26] E. H. Lieb and S. Oxford, Improved lower bound on the indirect coulomb energy, *Int. J. Quantum Chem.* **19**, 427 (1981).
- [27] X. Ren, P. Rinke, C. Joas, and M. Scheffler, Random-phase approximation and its applications in computational chemistry and materials science, *J. Mater. Sci. Lett.* **47**, 7447 (2012).
- [28] O. A. Vydrov and T. V. Voorhis, Nonlocal van der waals density functional: The simpler the better, *J. Chem. Phys.* **133**, 244103 (2010).
- [29] K. Berland and P. Hyldgaard, Exchange functional that tests the robustness of the plasmon description of the van der waals density functional, *Phys. Rev. B* **89**, 035412 (2014).
- [30] J. Řezáč, P. Jurečka, K. E. Riley, J. Černý, H. Valdes, K. Pluháčková, K. Berka, T. Řezáč, M. Pitoňák, J. Vondrášek, and P. Hobza, Quantum chemical benchmark energy and geometry database for molecular clusters and complex molecular systems (www.begdb.com): A users manual and examples, *Collect. Czech. Chem. Commun.* **73**, 1261 (2008).
- [31] J. Klimeš, D. R. Bowler, and A. Michaelides, Chemical accuracy for the van der waals density functional, *J. Phys.: Condens. Matter* **22**, 022201 (2009).
- [32] J. Klimeš, D. R. Bowler, and A. Michaelides, Van der waals density functionals applied to solids, *Phys. Rev. B* **83**, 195131 (2011).
- [33] H. Peng, Z.-H. Yang, J. P. Perdew, and J. Sun, Versatile Van Der Waals Density Functional Based on a Meta-Generalized Gradient Approximation, *Phys. Rev. X* **6**, 041005 (2016).
- [34] G. Kresse and J. Hafner, Ab initio molecular dynamics for liquid metals, *Phys. Rev. B* **47**, 558 (1993).
- [35] G. Kresse and J. Hafner, *Ab initio* molecular-dynamics simulation of the liquid-metal-amorphous-semiconductor transition in germanium, *Phys. Rev. B* **49**, 14251 (1994).
- [36] G. Kresse and J. Furthmüller, Efficiency of ab-initio total energy calculations for metals and semiconductors using a plane wave basis set, *Comput. Mater. Sci.* **6**, 15 (1996).

- [37] G. Kresse and J. Furthmüller, Efficient iterative schemes for *ab initio* total-energy calculations using a plane-wave basis set, *Phys. Rev. B* **54**, 11169 (1996).
- [38] P. E. Blöchl, Projector augmented-wave method, *Phys. Rev. B* **50**, 17953 (1994).
- [39] G. Kresse and D. Joubert, From ultrasoft pseudopotentials to the projector augmented-wave method, *Phys. Rev. B* **59**, 1758 (1999).
- [40] M. P. Teter, M. C. Payne, and D. C. Allan, Solution of schrödinger's equation for large systems, *Phys. Rev. B* **40**, 12255 (1989).
- [41] M. Methfessel and A. T. Paxton, High-precision sampling for brillouin-zone integration in metals, *Phys. Rev. B* **40**, 3616 (1989).
- [42] P. E. Blöchl, O. Jepsen, and O. K. Andersen, Improved tetrahedron method for brillouin-zone integrations, *Phys. Rev. B* **49**, 16223 (1994).
- [43] G. Kebede, P. D. Mitev, P. Broqvist, A. Eriksson, and K. Hermansson, Fifty shades of water: Benchmarking DFT functionals against experimental data for ionic crystalline hydrates, *J. Chem. Theory Comput.* **15**, 584 (2018).
- [44] E. J. Granhed, G. Wahnström, and P. Hyldgaard, BaZrO₃ stability under pressure: The role of nonlocal exchange and correlation, *Phys. Rev. B* **101**, 224105 (2020).
- [45] B. Vlasisavljević, J. Huck, Z. Hulvey, K. Lee, J. A. Mason, J. B. Neaton, J. R. Long, C. M. Brown, D. Alfè, A. Michaelides, and B. Smit, Performance of van der waals corrected functionals for guest adsorption in the m2(dobdc) metal-organic frameworks, *J. Phys. Chem. A* **121**, 4139 (2017).
- [46] Y. Yao and Y. Kanai, Plane-wave pseudopotential implementation and performance of SCAN meta-GGA exchange-correlation functional for extended systems, *J. Chem. Phys.* **146**, 224105 (2017).
- [47] A. H. Larsen, J. J. Mortensen, J. Blomqvist, I. E. Castelli, R. Christensen, M. Dułak, J. Friis, M. N. Groves, B. Hammer, C. Hargus, E. D. Hermes, P. C. Jennings, P. B. Jensen, J. Kermode, J. R. Kitchin, E. L. Kolsbjerg, J. Kubal, K. Kaasbjerg, S. Lysgaard, J. B. Maronsson, T. Maxson, T. Olsen, L. Pastewka, A. Peterson, C. Rostgaard, J. Schiøtz, O. Schütt, M. Strange, K. S. Thygesen, T. Vegge, L. Vilhelmsen, M. Walter, Z. Zeng, and K. W. Jacobsen, The atomic simulation environment—a python library for working with atoms, *J. Phys.: Condens. Matter* **29**, 273002 (2017).
- [48] A. Baldereschi, S. Baroni, and R. Resta, Band Offsets in Lattice-Matched Heterojunctions: A Model and First-Principles Calculations for GaAs/AlAs, *Phys. Rev. Lett.* **61**, 734 (1988).
- [49] C. J. Fall, N. Binggeli, and A. Baldereschi, Deriving accurate work functions from thin-slab calculations, *J. Phys.: Condens. Matter* **11**, 2689 (1999).
- [50] G. Wulff, XXV. zur frage der geschwindigkeit des wachstums und der auflösung der krystallflächen, *Z. Kristallogr. - Cryst. Mater.* **34**, 449 (1901).
- [51] J. Rahm and P. Erhart, WulffPack: A python package for wulff constructions, *J. Open Source Software* **5**, 1944 (2020).
- [52] See Supplemental Material at <http://link.aps.org/supplemental/10.1103/PhysRevB.102.075115> for two tables with structural, energetic, and electronic properties.
- [53] K. Lejaeghere, V. V. Speybroeck, G. V. Oost, and S. Cottenier, Error estimates for solid-state density-functional theory predictions: An overview by means of the ground-state elemental crystals, *Crit. Rev. Solid State Mater. Sci.* **39**, 1 (2013).
- [54] J. Bandyopadhyay and K. Gupta, Low temperature lattice parameter of nickel and some nickel-cobalt alloys and grüneisen parameter of nickel, *Cryogenics* **17**, 345 (1977).
- [55] P. Villars and J. Daams, Atomic-environment classification of the chemical elements, *J. Alloys Compd.* **197**, 177 (1993).
- [56] C. Han, S. Yang, K. G. Chang, P. P. Wang, R. ichi Murakami, and X. P. Song, Structure transition and magnetism of bcc-ni nanowires, *J. Mater. Chem. C* **3**, 1004 (2015).
- [57] M. Ohtake, M. Futamoto, and N. Inaba, Formation of bcc-ni thin film on GaAs(100) substrate and phase transformation from bcc to fcc, *Eur. Phys. J. B* **86** (2013).
- [58] C. S. Tian, D. Qian, D. Wu, R. H. He, Y. Z. Wu, W. X. Tang, L. F. Yin, Y. S. Shi, G. S. Dong, X. F. Jin, X. M. Jiang, F. Q. Liu, H. J. Qian, K. Sun, L. M. Wang, G. Rossi, Z. Q. Qiu, and J. Shi, Body-Centered-Cubic ni and its Magnetic Properties, *Phys. Rev. Lett.* **94**, 137210 (2005).
- [59] S. Jana, K. Sharma, and P. Samal, Assessing the performance of the recent meta-GGA density functionals for describing the lattice constants, bulk moduli, and cohesive energies of alkali, alkaline-earth, and transition metals, *J. Chem. Phys.* **149**, 164703 (2018).
- [60] G.-X. Zhang, A. M. Reilly, A. Tkatchenko, and M. Scheffler, Performance of various density-functional approximations for cohesive properties of 64 bulk solids, *New J. Phys.* **20**, 063020 (2018).
- [61] F. Tran, J. Stelzl, and P. Blaha, Rungs 1 to 4 of DFT jacob's ladder: Extensive test on the lattice constant, bulk modulus, and cohesive energy of solids, *J. Chem. Phys.* **144**, 204120 (2016).
- [62] W. Tyson and W. Miller, Surface free energies of solid metals: Estimation from liquid surface tension measurements, *Surf. Sci.* **62**, 267 (1977).
- [63] B. Baker, B. Johnson, and G. Maire, Photoelectric work function measurements on nickel crystals and films, *Surf. Sci.* **24**, 572 (1971).
- [64] A. Patra, J. E. Bates, J. Sun, and J. P. Perdew, Properties of real metallic surfaces: Effects of density functional semilocality and van der waals nonlocality, *Proc. Natl. Acad. Sci.* **114**, E9188 (2017).
- [65] P. Hyldgaard, Y. Jiao, and V. Shukla, Screening nature of the van der waals density functional method: A review and analysis of the many-body physics foundation, *J. Phys. Condens. Matter* **32**, 393001 (2020).
- [66] J. Avelar, A. Bruix, J. Garza, and R. Vargas, van der waals exchange-correlation functionals over bulk and surface properties of transition metals, *J. Phys.: Condens. Matter* **31**, 315501 (2019).
- [67] H. Meltzman, D. Chatain, D. Avizemer, T. M. Besmann, and W. D. Kaplan, The equilibrium crystal shape of nickel, *Acta Mater.* **59**, 3473 (2011).
- [68] J. P. Perdew, K. Burke, and M. Ernzerhof, Perdew, Burke, and Ernzerhof Reply:, *Phys. Rev. Lett.* **80**, 891 (1998).